

Spontaneous and field-induced magnetic phase transitions in $\text{Dy}_2\text{Co}_3\text{Al}_9$: Effects of exchange frustration

D. I. Gorbunov,¹ M. S. Henriques,^{2,3} N. Qureshi,² B. Ouladdiaf,² C. Salazar Mejía,¹ J. Gronemann,^{1,4}
A. V. Andreev,³ V. Petříček,³ E. L. Green,¹ and J. Wosnitza^{1,4}

¹*Hochfeld-Magnetlabor Dresden (HLD-EMFL), Helmholtz-Zentrum Dresden-Rossendorf, 01328 Dresden, Germany*

²*Institut Laue Langevin, 71 Avenue des Martyrs, F-38042 Grenoble, France*

³*Institute of Physics, Academy of Sciences, Na Slovance 2, 182 21 Prague, Czech Republic*

⁴*Institut für Festkörper- und Materialphysik, TU Dresden, 01062 Dresden, Germany*



(Received 17 June 2018; published 15 August 2018)

Due to the long-range oscillatory character of RKKY exchange interactions, for $\text{Dy}_2\text{Co}_3\text{Al}_9$ there exist positive and negative couplings between the Dy magnetic moments that lead to magnetic frustration. As a result, the ground state can be easily perturbed, and the system displays a number of spontaneous and field-induced phase transitions. We performed magnetization, magnetic-susceptibility, specific-heat, and electrical-resistivity measurements as well as neutron-diffraction experiments on a single crystal. We find two transitions to distinct incommensurate antiferromagnetic phases at 6.2 and 5.2 K that evolve to a commensurate phase at 3.7 K. In applied magnetic field, new phases emerge. Field-dependent magnetization exhibits a multistep metamagnetic process with sharp transitions accompanied by pronounced magnetoresistance changes. The large number of phases and their complex magnetic structures suggest that the physical properties of $\text{Dy}_2\text{Co}_3\text{Al}_9$ are ruled by exchange frustration in the presence of a large magnetocrystalline anisotropy.

DOI: [10.1103/PhysRevMaterials.2.084406](https://doi.org/10.1103/PhysRevMaterials.2.084406)

I. INTRODUCTION

$R_2T_3X_9$ compounds are a large class of materials that display a rich variety of electronic properties (R is a rare-earth element, Th or U; T is a d element; X is a p element). Magnetically ordered states, Pauli and Curie paramagnetism, mixed-valence, and Kondo-lattice behavior were reported [1–9]. Such different ground states are determined primarily by various hybridization strengths between the $3d$, $4d$, $4f$, $5f$ electrons and ligand atoms. This reflects that a fine balance among various contributions to the total energy is easily broken by elemental substitution, and a new ground state may be preferred.

$R_2T_3X_9$ compounds crystallize in the orthorhombic crystal structure of $\text{Y}_2\text{Co}_3\text{Ga}_9$ type [10–13]. As discussed [8,10,11], this structure is described as formed by two different types of slabs (Fig. 1). The A layer is composed of the R and X elements in the ratio $2R : 3X$. This slab is planar and corresponds to crystallographic mirror planes. The B layer contains the T and X elements in the relation $1T : 2X$, forming a nonplanar distorted triangular mesh. The perfect stacking is $ABA'B'$, where A' and B' correspond to mirror images of the A and B layers, respectively. The R atoms form a slightly distorted honeycomb network (A and A'), in which each R atom has two next-nearest neighbors at distances of 4.1 and 4.4 Å. These layers are separated by approximately 5.3 Å from the next neighboring R -containing layer by a layer composed of Co and Al (B and B').

Since the only symmetry position for the R atoms in $R_2T_3X_9$ is surrounded by 11 X ligand atoms, the physical properties of these compounds are strongly dependent on the type of the ligand atom. This point was demonstrated, e.g., for several Yb-

based systems containing Ga and Al [2,3,5]. In particular, the formation of magnetic order was reported for the Al-containing compounds $\text{Yb}_2\text{Co}_3\text{Al}_9$, $\text{Yb}_2\text{Rh}_3\text{Al}_9$, and $\text{Yb}_2\text{Ir}_3\text{Al}_9$, whereas their Ga-containing analogues are paramagnets down to the lowest temperatures.

Isotropic bilinear exchange interactions are mediated by conduction electrons [14]. These RKKY-type interactions are long-range and oscillatory with distance. The resulting competition between positive and negative couplings can frustrate magnetic moments. Magnetocrystalline anisotropy arises due to electrostatic interaction between the aspherical $4f$ charge cloud and the crystal electric field. This plays a dominant role in most of the physical properties associated with rare-earth magnetism. The crystal electric field can lock the rare-earth magnetic moment into a particular lattice direction. The interplay between competing oscillatory long-range RKKY-type exchange interactions in the presence of a large magnetocrystalline anisotropy can lead to unstable magnetic moments and complex magnetic states in $R_2T_3X_9$.

In the present paper, we investigate $\text{Dy}_2\text{Co}_3\text{Al}_9$. We find that with decreasing temperature, $\text{Dy}_2\text{Co}_3\text{Al}_9$ displays two distinct incommensurate antiferromagnetic phases that set in at 6.2 and 5.2 K before reaching a commensurate phase at 3.7 K. More phase transitions are found in applied magnetic field. Multistep metamagnetic transitions are observed along the principal crystallographic directions accompanied by pronounced magnetoresistance changes. The large number of phases and their complex magnetic structures reflect that the ground state can be easily perturbed and hint at an important role of frustration in the electronic properties of $\text{Dy}_2\text{Co}_3\text{Al}_9$.

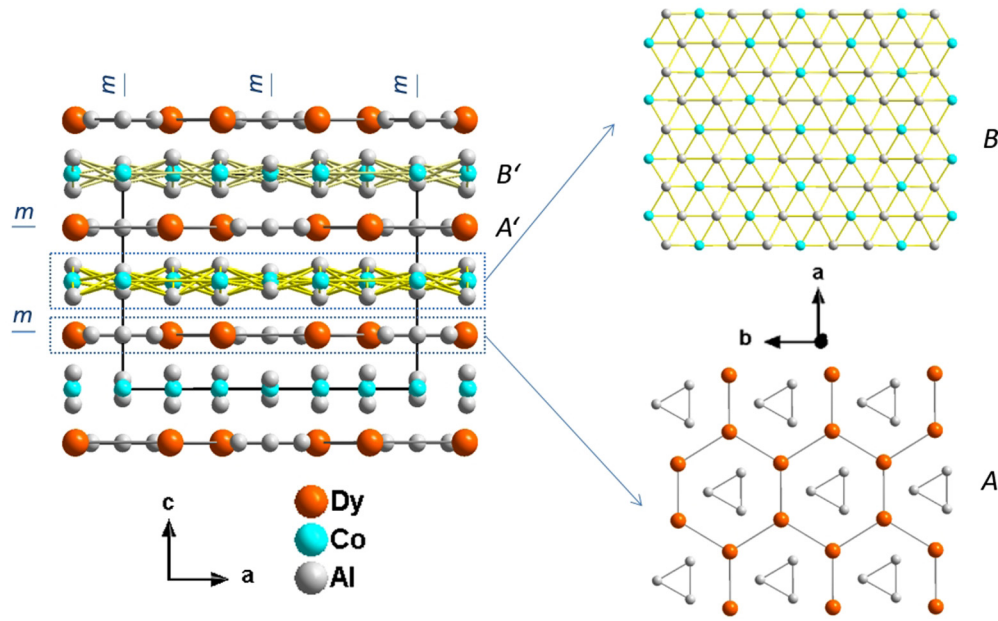


FIG. 1. Crystal structure of $\text{Dy}_2\text{Co}_3\text{Al}_9$. The unit cell (black line in the left panel) is projected onto the ac plane with the mirror planes shown by m . Two types of layers, A and B , are projected onto the ab plane on the right.

II. EXPERIMENTAL DETAILS

A $\text{Dy}_2\text{Co}_3\text{Al}_9$ single crystal was grown from a stoichiometric mixture of the pure elements (99.9% Dy, 99.99% Co, and 99.999% Al) by a modified Czochralski method in a tri-arc furnace under protective argon atmosphere. Back-scattered Laue diffraction patterns were used to check the single-crystalline state and to orient the crystal for magnetization, magnetic-susceptibility, electrical-resistivity, specific-heat, and neutron-scattering measurements. The Laue patterns show the high quality of the single crystal (see Supplemental Material [15]).

Single-crystal x-ray diffraction was used to determine the lattice parameters of $\text{Dy}_2\text{Co}_3\text{Al}_9$. The lattice parameters of the orthorhombic unit cell are $a = 12.7239(6)$ Å, $b = 7.4586(3)$ Å, and $c = 9.2994(5)$ Å at room temperature. Details on the data collection, refinement procedure, and final refinement factors are given in the Supplemental Material [15].

The temperature and field dependences of the magnetic susceptibility (frequency 97 Hz, excitation amplitude 0.001 T) and magnetization were measured along the principal crystallographic directions using a physical property measurement system PPMS-14 in static fields up to 14 T between 2 and 300 K. The PPMS was also used to measure electrical resistivity by the four-point method with an excitation current of $I = 5$ mA flowing along the c axis.

Specific heat was measured in a ^3He cryostat using the continuous-relaxation method. The sample was affixed to a sapphire platform with a small amount of grease. After heating the sample and platform by 400 to 500%, the heater was turned off and the cooldown of the sample was recorded. Specific heat was calculated as described in Ref. [16].

The magnetization in pulsed magnetic fields up to 57 T (pulse duration 25 ms) was measured at the Dresden High Magnetic Field Laboratory. The high-field magnetometer is

described in Ref. [17]. Absolute values of the magnetization were calibrated using data from static-field measurements.

The reciprocal space of the $\text{Dy}_2\text{Co}_3\text{Al}_9$ single crystal was first explored by neutron Laue diffraction using the CYCLOPS (CYlindrical Ccd Laue Octagonal Photo Scintillator) instrument at the Institute Laue-Langevin (ILL) [18]. The crystal was fixed and inserted in an aluminum cylinder and cooled to 15 K at a rate of 1 K/min. During the cooling, one Laue image per minute was recorded. The temperature was then stabilized at 15 K and a set of 36 images was taken. These images were corrected and averaged to produce a unique Laue pattern. This procedure was repeated at 5.8, 4.5, and 1.5 K. The nuclear reflections from the Laue pattern taken at 15 K were indexed using the program Esmeralda Laue Suite [19]. The magnetic reflections were used to determine the components of the propagation vector of the different magnetic phases.

In order to solve the magnetic structures, further neutron-scattering experiments were performed using the four-circle diffractometer D10 at ILL (incident neutron wavelength of $\lambda = 2.36$ Å, using a pyrolytic graphite monochromator). A small set of strong and well-centered nuclear reflections was used to orient the single crystal. The intensities of larger sets of reflections were collected in the paramagnetic phase (at 15 K) and within each antiferromagnetic phase (at 5.8, 4.5, and 1.5 K). Temperature scans were also performed between 2 and 8 K. The nuclear and magnetic structures of $\text{Dy}_2\text{Co}_3\text{Al}_9$ were solved employing the program Jana2006 [20,21]. Further details on the neutron-data refinements can be found in Tables S4, S5, and S6 in the Supplemental Material [15]. For a better analysis and description of the magnetic structures, we have also used some of the computational tools available at the Bilbao Crystallographic Server, namely in its section of Magnetic Symmetry and Applications (MVISUALIZE, k-SUBGROUPSMAG, and MAGNEXT) [22].

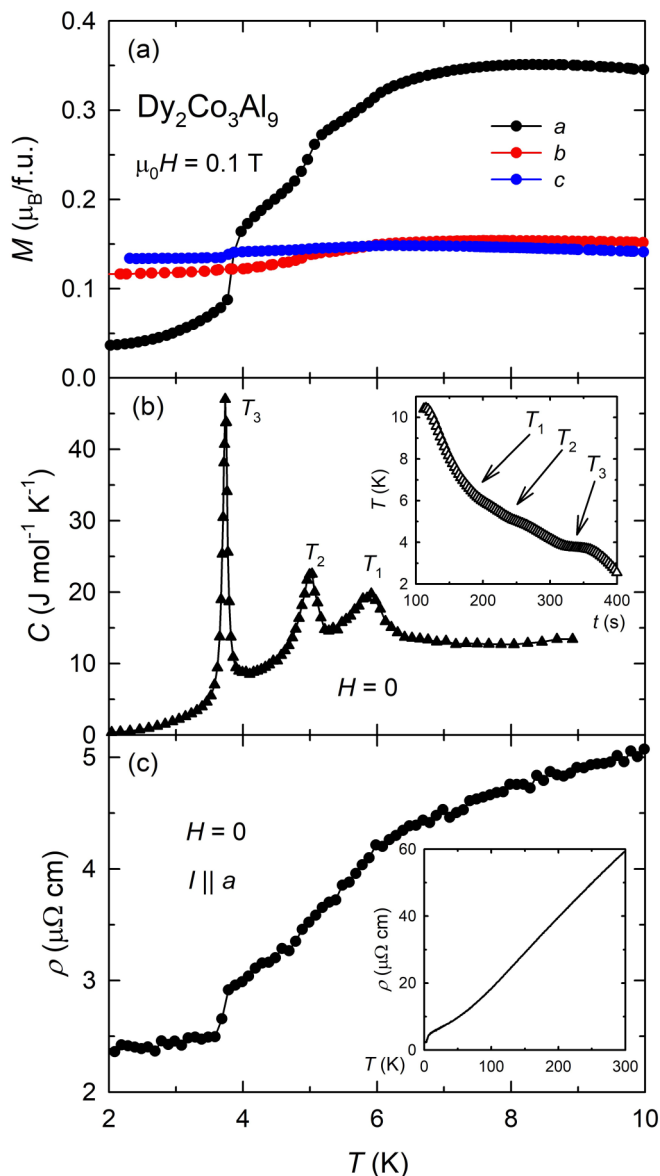


FIG. 2. Temperature dependences of (a) the magnetization, M , for a field of 0.1 T applied along the a , b , and c axes; (b) the specific heat, C ; and (c) the electrical resistivity, ρ , of $\text{Dy}_2\text{Co}_3\text{Al}_9$. The inset in panel (b) shows a temperature-time, T - t , relaxation curve. The inset in panel (c) shows, ρ , between 2 and 300 K.

III. RESULTS

$\text{Dy}_2\text{Co}_3\text{Al}_9$ displays magnetic order at low temperatures. To obtain information about the ordered state, we measured temperature dependences of the magnetization, M , specific heat, C , and electrical resistivity, ρ . The $M(T)$ dependence in a field of 0.1 T applied along the a axis displays three anomalies: an inflection point around 6 K, a shoulder around 5 K, and a step just below 4 K [Fig. 2(a)]. The magnetization for field applied along the b and c axes is less sensitive to changes in the magnetic order. The b -axis magnetization increases somewhat between 4 and 6 K, while the c -axis magnetization exhibits a small step below 4 K. The magnetic susceptibility of $\text{Dy}_2\text{Co}_3\text{Al}_9$ up to 300 K can be found in the Supplemental Material [15].

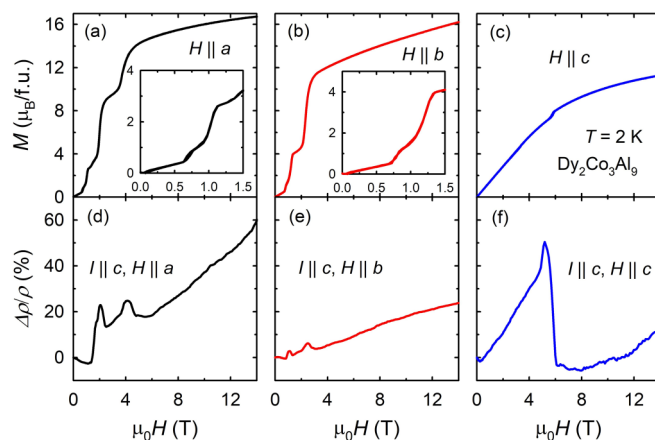


FIG. 3. Magnetization and magnetoresistance measured for fields applied along the a [(a) and (d)], b [(b) and (e)], and c axes [(c) and (f)] of $\text{Dy}_2\text{Co}_3\text{Al}_9$ at 2 K. The insets in panels (a) and (b) show an enlarged view of the magnetization at low fields.

The specific heat provides information on the temperature and type of the observed phase transformations. Figure 2(b) indicates that the two phase transitions at $T_1 = 6.2(2)$ K and $T_2 = 5.2(2)$ K are of second order, whereas the transition observed at $T_3 = 3.7(1)$ K is of first order. Evidence for the first- and second-order type of the observed transitions is given by a temperature-time relaxation curve [inset in Fig. 2(b)]. The second-order transitions are identified through inflection points, whereas the first-order transition causes a plateau, which is a feature of transitions involving latent heat.

The electrical resistivity displays a metallic character [inset in Fig. 2(c)]. At 2 K, $\rho = 2.4 \mu\Omega \text{ cm}$. The residual resistivity ratio between 300 and 2 K is $\frac{60.5}{2.4} \approx 25$. ρ is affected by the onset of the antiferromagnetic ordering where ρ exhibits an inflection point. No anomalies in ρ can be resolved at T_2 . The first-order transition at T_3 causes a step in $\rho(T)$ as in the magnetization [Fig. 2(a)].

The type of magnetic order can be inferred from field-dependent magnetization data [Figs. 3(a)–3(c)]. At 2 K, $\text{Dy}_2\text{Co}_3\text{Al}_9$ displays no spontaneous magnetic moment as can be expected for an antiferromagnetic state. We also measured magnetization isotherms between 2 and 6 K (not shown), i.e., in the other two magnetically ordered phases, and also observed zero spontaneous magnetic moment. We conclude that the three phases of $\text{Dy}_2\text{Co}_3\text{Al}_9$ below T_1 are antiferromagnetically ordered. This result contradicts an earlier work where $\text{Dy}_2\text{Co}_3\text{Al}_9$ was reported to be ferromagnetic on the basis of a magnetic-susceptibility measurement of a polycrystal [4].

$\text{Dy}_2\text{Co}_3\text{Al}_9$ shows complex field-dependent magnetization. For fields up to 14 T applied along the a axis, four field-induced magnetic phase transitions are observed [three jumps can be seen at 1.1, 2, and 3.9 T in Fig. 3(a); an additional small jump at 0.7 T can be seen in the inset in Fig. 3(a)]. When the field is applied along the b axis, three magnetization jumps occur [at 1.2 and 2.4 T in Fig. 3(b); at 0.8 T in the inset in Fig. 3(b)]. A field-induced transition is also observed at 5.8 T for field applied along the c axis. The observed field-induced anomalies are likely related to rotations of the magnetic moments and crystal-electric-field (CEF) effects [23–27].

In the highest field of 14 T, the magnetization exceeds $16 \mu_B/\text{f.u.}$ for fields applied along the a and b axes and approaches $11 \mu_B/\text{f.u.}$ for field applied along the c axis. This is lower than the value expected if the full magnetic moments, $M_{\text{Dy}} = 10 \mu_B$, of the Dy atoms contribute to the magnetization: $2 \times M_{\text{Dy}} = 20 \mu_B$. However, M_{Dy} might be reduced at 2 K. This temperature is relatively “high” since $\text{Dy}_2\text{Co}_3\text{Al}_9$ becomes paramagnetic at 6 K. The Co atoms are polarized by the applied field and might also develop an ordered magnetic moment. With increasing temperature, the transitions broaden and disappear (not shown).

As the field-dependent magnetization of $\text{Dy}_2\text{Co}_3\text{Al}_9$ continues to increase up to 14 T, we measured $M(H)$ dependences in pulsed magnetic fields up to 57 T (see Supplemental Material [15]). No additional phase transitions are observed up to the highest field.

The magnetic field strongly affects as well the electrical resistivity of $\text{Dy}_2\text{Co}_3\text{Al}_9$, especially at the field-induced phase transitions [Figs. 3(d)–3(f)]. Most of the magnetization jumps are accompanied by peaks in the magnetoresistance, $\Delta\rho/\rho$. For field applied along the a axis, the first two transitions do not affect $\Delta\rho/\rho$ much. However, as the magnetization change at the transition increases, the magnetoresistance grows and exceeds 20% for the last two jumps. A similar situation occurs for field applied along the b axis. The low-field jump does not influence the resistivity much but the transitions at higher fields are accompanied by positive $\Delta\rho/\rho$. The largest effect is observed for field applied along the c axis. Although the magnetization jump is rather small, it leads to a sharp maximum and a large negative magnetoresistance that drops by 53%. In fields above the field-induced transitions, the magnetoresistance increases for all field orientations.

Large magnetoresistance changes suggest that the conduction electrons strongly interact with the localized magnetic moments of $\text{Dy}_2\text{Co}_3\text{Al}_9$. At the field-induced transitions, domains with various magnetic-moment orientations coexist within the sample (see, e.g., Ref. [28]). An additional contribution to the electrical resistivity might be due to scattering of conduction electrons on magnetic moments distributed in phase boundaries that play the role of magnetic defects. However, this is unlikely to be the dominant mechanism since $\text{Dy}_2\text{Co}_3\text{Al}_9$ exhibits a large magnetic anisotropy that makes domain walls narrow so that their volume fraction is likely to be small in the sample.

A more likely reason for the observed peaks in $\Delta\rho/\rho$ is different conduction electron spectra in phases with different magnetic structures [29]. The difference in the interaction between the conduction and f electrons in different magnetic phases can give rise to a potential barrier at the phase boundary. If the Fermi energy is larger than the potential barrier, the electrons pass from one phase into the other. Otherwise, the electrons are reflected, which increases the resistivity. Pronounced peaks were also observed in the magnetoresistance of ErGa_2 , Tb_3Co , Dy_3Co , RNiGe_3 , and $\text{R}_3\text{Ru}_4\text{Al}_{12}$ [29–33].

To map out the T - H phase diagram of $\text{Dy}_2\text{Co}_3\text{Al}_9$, we performed specific-heat measurements in magnetic fields (Fig. 4). Our data show that in fields up to 2 T new phase transitions emerge. For clarity, all anomalies in Fig. 4 are labeled. However, it is hard to attribute some anomalies to specific phase transitions. With increasing field, the anomalies at T_2 and T_3 shift to lower temperatures, whereas the paramagnetic-

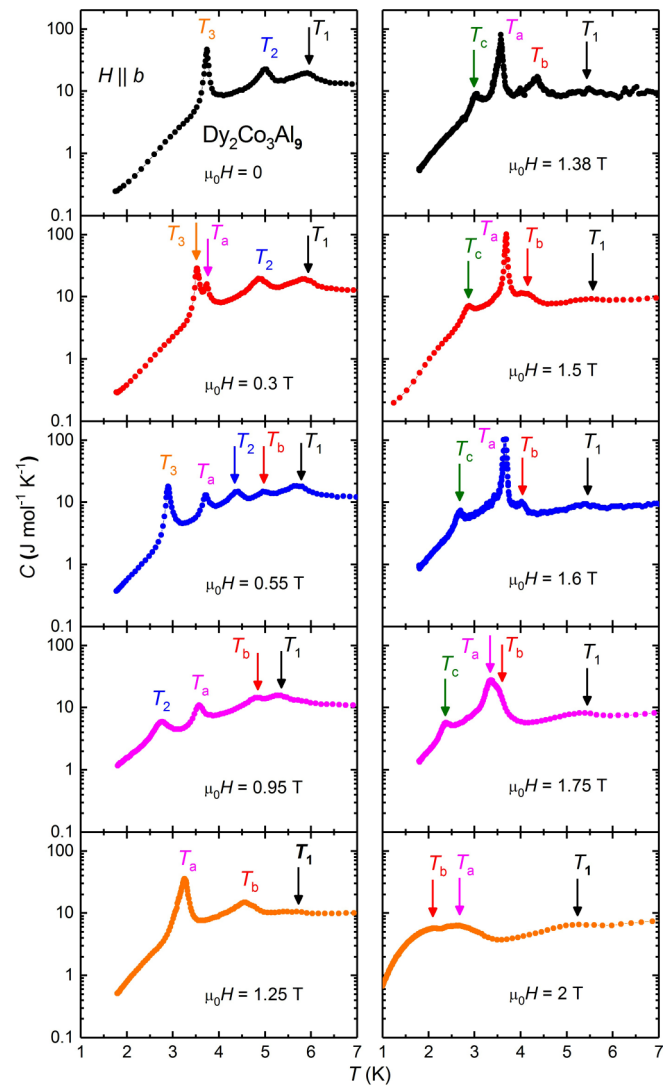


FIG. 4. Temperature dependences of the specific heat in fields up to 2 T applied along the b axis of $\text{Dy}_2\text{Co}_3\text{Al}_9$.

antiferromagnetic phase transition at T_1 is much less affected up to 2 T. The first-order phase transition is not observed above 0.55 T, and the transition at T_2 disappears in the vicinity of 1 T. At 0.3 T, a new second-order anomaly emerges at $T_a = 3.8 \pm 0.1$ K. Initially, the field shifts this transition to lower temperatures. Between 1.25 and 1.75 T, it appears to be of first order. At 2 T, a broad anomaly indicates that it is again of second order. Two more phase transitions, absent in zero field, emerge at 0.55 T at $T_b = 5.1 \pm 0.1$ K and at 1.38 T at $T_c = 3.3 \pm 0.2$ K.

The H - T phase diagram of $\text{Dy}_2\text{Co}_3\text{Al}_9$ is shown in Fig. 5. The critical temperatures T_2 , T_3 , T_b , and T_c decrease monotonously with increasing field, whereas T_a and T_1 change much less in applied field. A microscopic study such as neutron scattering is required to obtain more detailed information on the field-induced phases.

Our macroscopic measurements point out that $\text{Dy}_2\text{Co}_3\text{Al}_9$ provides an opportunity to study the interplay among exchange interactions, magnetocrystalline anisotropy, and possible magnetic frustration. The free energies of adjacent magnetic

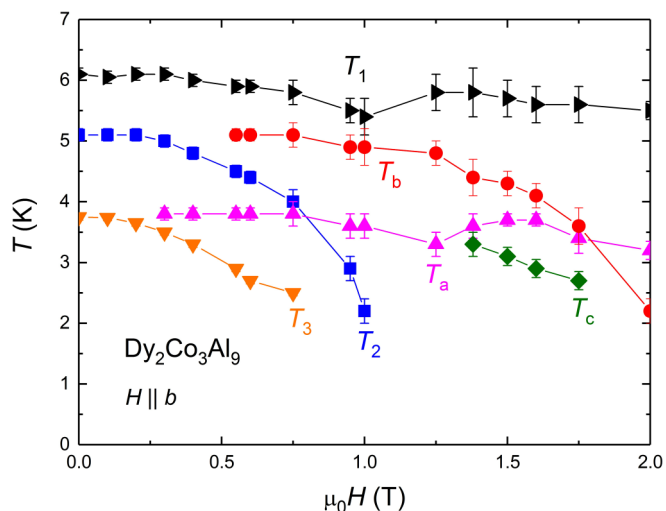


FIG. 5. Phase diagram of $\text{Dy}_2\text{Co}_3\text{Al}_9$ in magnetic fields up to 2 T applied along the b axis.

states are nearly degenerated, and the compound can be driven into a different phase by small changes in temperature and magnetic field. For rare-earth-based intermetallic compounds, exchange interactions of the RKKY-type often lead to incommensurate magnetic structures that change to simpler, generally commensurate magnetic structures at lower temperatures [34,35]. Thus, $\text{Dy}_2\text{Co}_3\text{Al}_9$ is a good candidate for studies of magnetic structures and their changes through phase transformations.

A small region of the Laue diffraction images taken from a $\text{Dy}_2\text{Co}_3\text{Al}_9$ single crystal at different temperatures is shown in Fig. 6. At 15 K, all strong nuclear reflections could be indexed in the orthorhombic $Cmcm$ space group with lattice parameters $a = 12.7200 \text{ \AA}$, $b = 7.4391 \text{ \AA}$, and $c = 9.3042 \text{ \AA}$. The strongest nuclear reflections are accompanied by a weaker neighboring reflection due to the presence of a small twinned crystal [Fig. 6, upper panel, e.g., reflection (1 -1 2)]. Nevertheless, its presence does not hamper the full indexation of the diffraction pattern. When ramping the temperature down to 1.5 K and thus crossing different transition temperatures, new reflections appear at different positions in the reciprocal space below each transition temperature.

The magnetic structure factors derived from the kinematic theory of diffraction [36] describe the position and intensity of the diffraction spots in reciprocal space. They are localized at diffraction points, $\mathbf{g} = \mathbf{h} \pm m\mathbf{k}$, where \mathbf{k} is the characteristic propagation vector of the magnetic phase and m is the order of the reflection. That is, each reflection of the basic structure \mathbf{g} is surrounded by a series of equally spaced satellite reflections at distances $\pm m\mathbf{k}$ from the main reflection described by the diffraction vector, \mathbf{h} .

In the present case, the propagation vectors of the magnetic structures of $\text{Dy}_2\text{Co}_3\text{Al}_9$ were found to be $\mathbf{k}_1 = (0, 0.13, 1)$ at 5.8 K, $\mathbf{k}_2 = (0, 0.06, 0.26)$ at 4.5 K, and $\mathbf{k}_3 = (0, 0, 0.5)$ at 1.5 K. Thus, the magnetic phases at 5.8 and 4.5 K are incommensurate modulated structures, as described by \mathbf{k}_1 and \mathbf{k}_2 , for which only first-order satellites were observed. The magnetic structure is commensurate with the crystal lattice at 1.5 K.

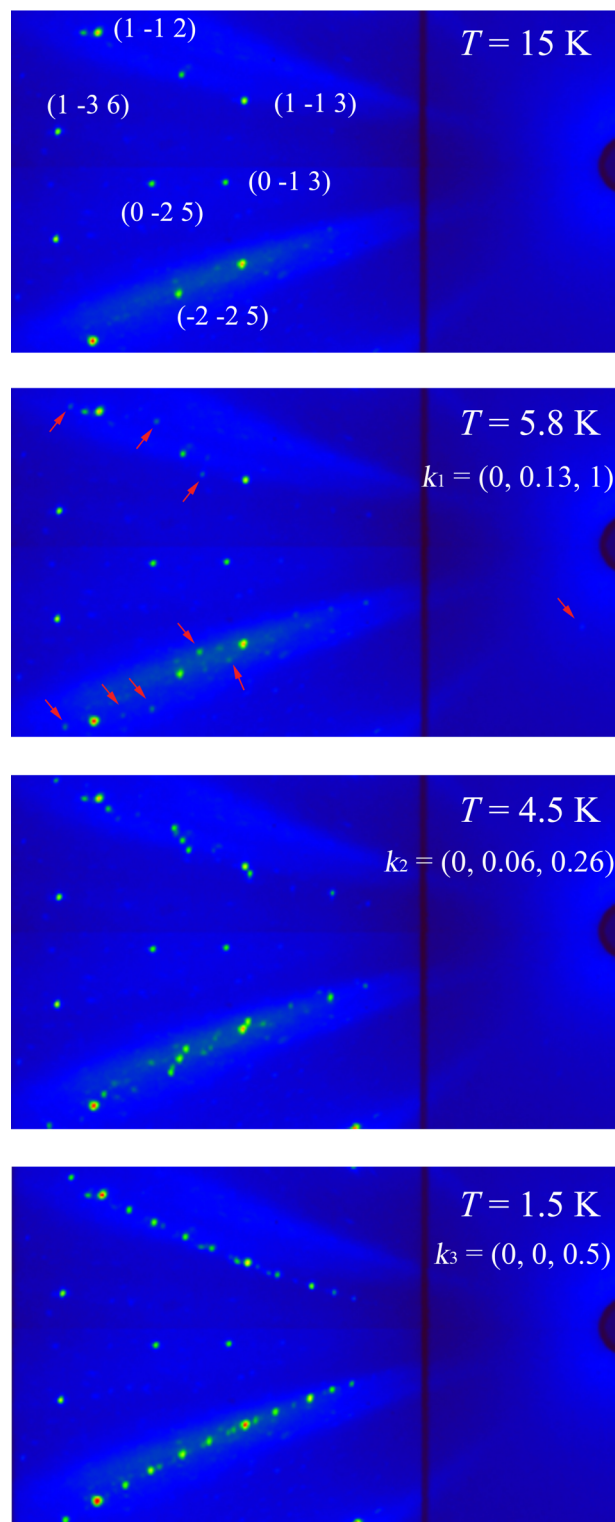


FIG. 6. Laue diffraction images of the $\text{Dy}_2\text{Co}_3\text{Al}_9$ single crystal taken at 15, 5.8, 4.5, and 1.5 K. At 15 K, some of the nuclear Bragg reflections are indexed as a reference. Magnetic satellites are present within the different magnetic phases and the respective propagation vectors, \mathbf{k}_i ($i = 1, 2, 3$ for 5.8, 4.5, and 1.5 K, respectively), as stated in the panels. The magnetic reflections are weaker at 5.8 K and are indicated by red arrows. The intensity of the magnetic reflections increases progressively with decreasing temperature.

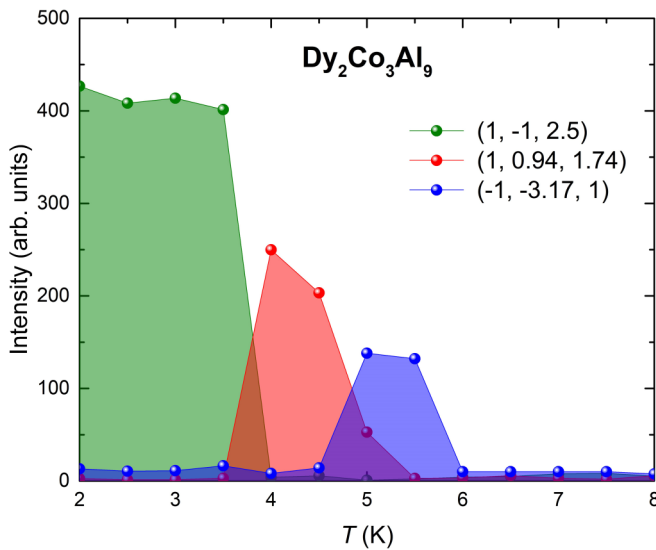


FIG. 7. Temperature dependences of the integrated intensities of selected magnetic reflections of $\text{Dy}_2\text{Co}_3\text{Al}_9$.

Figure 7 displays the integrated intensity of several magnetic reflections of $\text{Dy}_2\text{Co}_3\text{Al}_9$ as a function of temperature, showing the temperature regions where each magnetic phase is thermodynamically stable. These temperature ranges are in good agreement with those determined from magnetization, electrical-resistivity, and specific-heat measurements (see Fig. 2). There seems to be a narrow temperature region, $4.5 \leq T \leq 5.5$ K, where the two incommensurate phases coexist. It can also be seen that the intensity of the magnetic satellites is weaker for $(-1, -3.17, 1)$ and $(1, 0.94, 1.74)$ than for $(1, -1, 2.5)$, as was already observed in the Laue images (see Fig. 6).

Using the analysis and refinement tools implemented in Jana2006, we were able to assign magnetic superspace groups that describe the incommensurate magnetic structures at 5.8 and 4.5 K. The resulting Fourier sine and cosine amplitudes for the symmetry-independent Dy atoms are listed in Table S4 in the Supplemental Material [15]. Details of the refinement and comparison between different magnetic superspace models are listed in Table S5 in the Supplemental Material [15].

At 5.8 K, the configuration of the magnetic moments is given by the magnetic superspace group $Cmcm1'(0\beta 1)s0ss$. This group corresponds to an active primary two-dimensional irreducible representation (*irrep*), $mDT2$ (\mathbf{k}_1 is part of the DT line of the Brillouin zone). The magnetic structure is shown in Fig. 8. It can be described as an elliptical oblique cycloid. That is, the magnetic moments describe an elliptical rotation in the ab plane [Figs. 8(a) and 8(b)], with the spiral rotation direction parallel to the b axis. The largest moment of $3.3(1) \mu_B/\text{Dy}$ atom is tilted by an angle $\phi \approx 11(1)^\circ$ from the a axis [Fig. 8(c)]. The smallest moment is $1.9(2) \mu_B/\text{Dy}$ atom. The phase difference between two consecutive spins is close to 45° . The Dy atom keeps its special position, so that its spin components are forced by symmetry to be in-plane (see Table S4 in the Supplemental Material [15]). The point-group symmetry of this structure is $mmm1'$, so that the magnetic order does not break the symmetry of the system when compared to the parent symmetry. In fact, the spin cycloids keep the space inversion by symmetry-related cycloids of opposite chirality as given by the symmetry operators of the magnetic superspace group.

For the magnetic structure at 4.5 K, the best solution for the magnetic structure was found in the magnetic superspace group $C2/m1'(0\beta\gamma)0ss$. In this case, the corresponding active two-dimensional *irrep* is $mK2$ (\mathbf{k}_2 is part of the K plane of the Brillouin zone). As shown in Fig. 9, the magnetic structure can be seen as a collinear transverse oblique spin

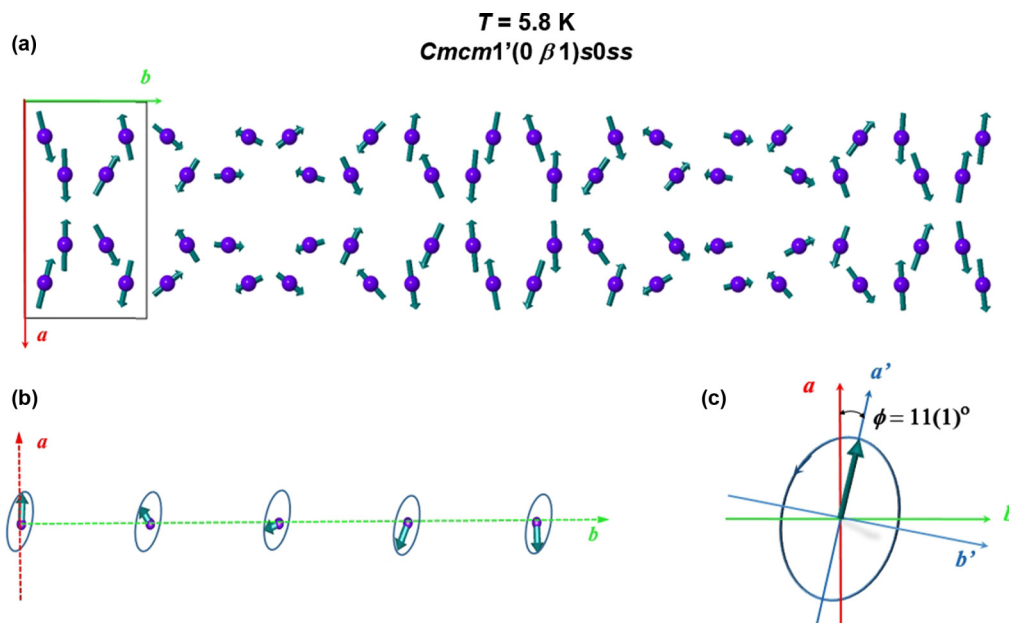


FIG. 8. Magnetic structure of $\text{Dy}_2\text{Co}_3\text{Al}_9$ at 5.8 K: (a) The Dy atoms (purple spheres) and respective magnetic moments (green arrows) are extended in a $1 \times 8 \times 1$ supercell of the parent orthorhombic unit cell (gray lines); (b) the magnetic moments describe an elliptical rotation in the ab plane that propagates along the b axis; (c) the largest moment is inclined from the a axis by an angle $\phi = 11(1)^\circ$.

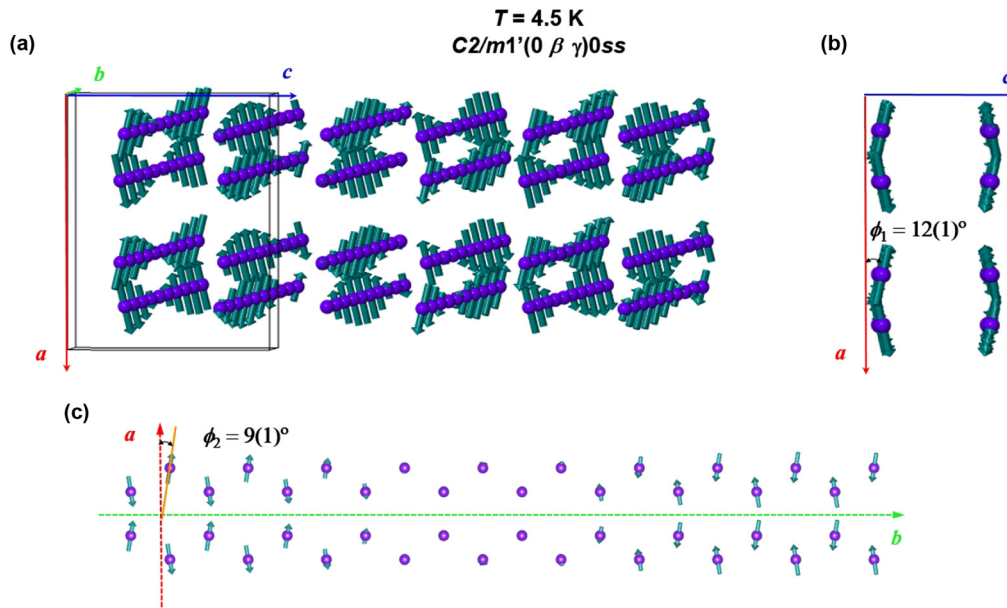


FIG. 9. Magnetic structure of $\text{Dy}_2\text{Co}_3\text{Al}_9$ at 4.5 K: (a) The Dy atoms (purple spheres) and their magnetic moments (green arrows) are extended in a $1 \times 5 \times 1$ supercell of the parent orthorhombic unit cell (gray lines); (b) the magnetic moments describe a collinear transverse oblique spin wave that propagates parallel to the b axis. The spin wave is inclined at angles $\phi_1 = \pm 12(1)^\circ$ towards the ab plane; (c) within the ab plane, the magnetic moments are inclined from the a axis at an angle $\phi_2 = \pm 9(1)^\circ$.

wave that propagates along the b axis. The magnetic moments lie in planes at angles $\phi_1 = \pm 12(1)^\circ$ away from the ab plane [Fig. 9(b)], and are inclined by $\phi_2 = 9(1)^\circ$ away from the a axis [Fig. 9(c)]. In this case, there is a break in the point-group symmetry from $mmm1'$ to $2/m1'$, but the space inversion is conserved. The magnetic modulation does not split the atomic site of the Dy atom, but it is now at a general position and its spin components have no symmetry restrictions. Furthermore, the collinearity of the spins is not symmetry protected and more complex phase relations are possible under this magnetic superspace group/*irrep*. In order to check this structure and avoid false minima, other runs were performed randomizing automatically the spin components of the Dy atom in Jana2006. Details of the refinements are given in Table S5 in the Supplemental Material [15].

For the data collected at 1.5 K, the representation analysis indicates that there are four maximal space groups of the gray group $Cmcm1'$ compatible with the \mathbf{k}_3 propagation vector (see Table S6 in the Supplemental Material [15]). The model that fits best our experimental data at this temperature is given by the maximal noncentrosymmetric magnetic space group, A_2mm2 . This spin arrangement complies with the two-dimensional *irrep* $mZ1$ (\mathbf{k}_3 is at the point Z in the Brillouin zone) restricted to the order-parameter direction $(0, a)$. The Dy position is now split into two different orbits, which have different symmetry-protected degrees of freedom for the spin components. One of the positions allows noncollinear magnetic moments parallel to the ab plane, whereas the other restricts the magnetic moments to be collinear and oriented along the c axis. The magnetic unit cell of $\text{Dy}_2\text{Co}_3\text{Al}_9$ is obtained by alternating these two types of configurations along the c axis, as shown in Fig. 10. The larger Dy moment is found along the b axis. It amounts to $8.4(1) \mu_B/\text{Dy}$ atom and lies at angles of $\pm 81(1)^\circ$ away from the a axis. Our data show that the Co atoms do

not carry an ordered magnetic moment at any temperature in $\text{Dy}_2\text{Co}_3\text{Al}_9$.

IV. DISCUSSION AND CONCLUSION

The magnetic properties of $\text{Dy}_2\text{Co}_3\text{Al}_9$ are ruled by exchange interactions and magnetocrystalline anisotropy. Our macroscopic measurements show that the ground state can be easily perturbed by small changes in temperature and magnetic field. This is corroborated by our neutron-diffraction study that revealed two distinct incommensurate and one commensurate phase between 1.5 and 6.2 K in zero field.

Cobalt does not carry an ordered magnetic moment in $\text{Dy}_2\text{Co}_3\text{Al}_9$. This could be guessed already from the relatively low magnetic ordering temperature and was proven by our neutron-diffraction data. This finding is surprising since Co is usually a source of strong exchange interactions in R - T intermetallic compounds (see, e.g., Ref. [37]). The nonmagnetic state of Co can likely be explained by the band structure of $\text{Dy}_2\text{Co}_3\text{Al}_9$. The $3d$ band might be too broad leading to a low density of states at the Fermi level. As a result, splitting of the $3d$ band does not occur. The nonmagnetic state of Co makes it possible to consider only the Dy magnetic moments in the discussion below.

The nearly degenerate free energies of adjacent magnetic phases can be explained by frustration effects. A geometric frustration is not given in $\text{Dy}_2\text{Co}_3\text{Al}_9$ as can be concluded from the hexagonal arrangement of the Dy atoms in the ab plane (see Fig. 1). Therefore, exchange (or bond) frustration is likely to play the key role.

The only relevant exchange interactions for $\text{Dy}_2\text{Co}_3\text{Al}_9$ are of RKKY type, which are long-range and oscillatory with distance. This results in positive and negative interionic couplings that frustrate the Dy magnetic moments. The existence of

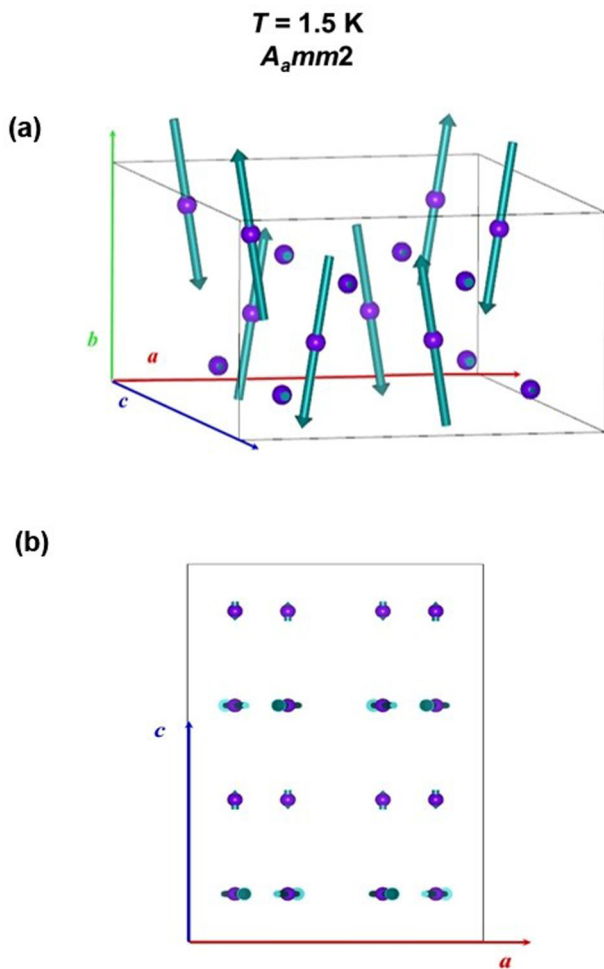


FIG. 10. Magnetic structure of $\text{Dy}_2\text{Co}_3\text{Al}_9$ at 1.5 K: (a) The Dy atoms (purple spheres) and their magnetic moments (green arrows) are shown in a $1 \times 1 \times 2$ cell of the parent orthorhombic unit cell (gray lines); (b) view of the magnetic unit cell along the b axis.

magnetic order reflects other, possibly weaker but nevertheless non-negligible contributions to the free energy, such as the interaction of the CEF with the $4f$ moments (magnetocrystalline anisotropy), quadrupolar interaction, magnetoelastic coupling, etc. More insight into the physics of $\text{Dy}_2\text{Co}_3\text{Al}_9$ can be gained by studying CEF effects.

In fact, the existence of an amplitude-modulated magnetic structure between 5.2 and 3.7 K suggests a large magnetic anisotropy for $\text{Dy}_2\text{Co}_3\text{Al}_9$ comparable with the leading magnetic exchange (the Weiss temperature is $\theta = +16$ K for field

applied along the a axis, see Table S3 in the Supplemental Material [15]). The anisotropy forces the moments along a given crystal direction, although their amplitudes are sinusoidally modulated. For weak or planar anisotropy, helimagnetic structures are usually observed for rare-earth-based intermetallic compounds [35]. At 3.7 K, the periodicity changes to another one with a shorter magnetic unit cell.

A transition from an amplitude-modulated incommensurate magnetic structure just below T_N to a commensurate structure at a lower temperature is common in intermetallic compounds based on rare-earth elements [34,35]. From the viewpoint of magnetic entropy, it is unfavorable for a doublet ground state to have zero magnetic moments for some sites. The transition to a commensurate magnetic structure is a result of a compromise between the exchange interactions and magnetic anisotropy that favors large magnetic moments upon approaching zero temperature.

Our findings for $\text{Dy}_2\text{Co}_3\text{Al}_9$ compare well with other groups of rare-earth-based intermetallic compounds. Incommensurate magnetic structures were reported for, e.g., $\text{NdNi}_{1-x}\text{Cu}_x$ with $x = 0.8 - 1$ [38], $R\text{Co}_2\text{Ge}_2$ with $R = \text{Tb}, \text{Dy},$ and Ho [39,40], Ho_2RhIn_8 [41], and $\text{Er}_2\text{Ni}_2\text{Pb}$ [42]. These long-period structures change to commensurate phases with decreasing temperature. Interestingly, for the compounds containing $3d$ elements, Co and Ni do not carry an ordered magnetic moment, similarly to Co for $\text{Dy}_2\text{Co}_3\text{Al}_9$.

In conclusion, our macro- and microscopic measurements suggest the presence of frustration effects in $\text{Dy}_2\text{Co}_3\text{Al}_9$ due to the existence of competing exchange interactions in the presence of a large magnetocrystalline anisotropy. The antiferromagnetic ground state can be easily perturbed by small changes in temperature and magnetic field, resulting in a complex phase diagram. Due to the nonmagnetic state of Co, the analysis of the physical properties of $\text{Dy}_2\text{Co}_3\text{Al}_9$ is simplified, and magnetic and other electronic properties associated with the localized $4f$ moments can be studied directly. Thus, our results show that $R_2\text{Co}_3\text{Al}_9$ compounds with magnetic R elements are ideally suited to study effects of exchange frustration.

ACKNOWLEDGMENTS

Part of the work was supported by the project 16-03593S of the Czech Science Foundation. This work was partly performed in the Materials Growth and Measurement Laboratory (MGML, <https://mgml.eu>). We acknowledge the support of HLD at HZDR, member of the European Magnetic Field Laboratory (EMFL). M.S.H. also acknowledges the Project No. LO1603 under the Ministry of Education, Youth and Sports National sustainability programme I of Czech Republic.

- [1] R. A. Gordon, F. J. DiSalvo, R. Pöttgen, and N. E. Brese, *Faraday Trans.* **92**, 2167 (1996).
- [2] S. K. Dhar, C. Mitra, P. Manfrinetti, A. Palenzona, and P. Bonville, *Physica B* **259-261**, 150 (1999).
- [3] O. Trovarelli, C. Geibel, B. Buschinger, R. Borth, S. Mederle, M. Grosche, G. Sparn, F. Steglich, O. Brosch, and L. Donnevert, *Phys. Rev. B* **60**, 1136 (1999).

- [4] C. Routsis and J. K. Jakinthos, *J. Alloys Compd.* **323-324**, 427 (2001).
- [5] T. Okane, S. I. Fujimori, A. Ino, A. Fujimori, S. K. Dhar, C. Mitra, P. Manfrinetti, A. Palenzona, and O. Sakai, *Phys. Rev. B* **65**, 125102 (2002).
- [6] O. Sichevych, W. Schnelle, Y. Prots, U. Burkhardt, and Y. Grin, *Z. Naturforsch. Sect. B - A J. Chem. Sci.* **61**, 904 (2006).

- [7] O. Tougait and H. Noël, *J. Alloys Compd.* **417**, 1 (2006).
- [8] J. Niermann, B. Fehrmann, M. W. Wolff, and W. Jeitschko, *J. Solid State Chem.* **177**, 2600 (2004).
- [9] R. Troć, O. Tougait, and H. Noël, *Intermetallics* **15**, 1091 (2007).
- [10] Y. N. Grin', R. E. Gladyshevskii, O. M. Sichevich, V. E. Zavodnik, Y. P. Yarmolyuk, and I. V. Rozhdestvenskaya, *Sov. Phys. Crystallogr.* **29**, 528 (1984).
- [11] R. E. Gladyshevskii, K. Cenzual, and E. Parthé, *J. Alloys Compd.* **182**, 165 (1992).
- [12] M. Schlüter and W. Jeitschko, *Z. Anorg. Allg. Chem.* **626**, 2217 (2000).
- [13] Y. Lutsyshyn, Y. Tokaychuk, and R. Gladyshevskii, *Chem. Met. Alloys* **4**, 243 (2011).
- [14] I. A. Campbell, *J. Phys. F: Met. Phys.* **2**, L47 (1972).
- [15] See Supplemental Material at <http://link.aps.org/supplemental/10.1103/PhysRevMaterials.2.084406> for additional experimental data (Laue diffraction patterns, details of the refinement of x-ray data, magnetic susceptibility, high-field magnetization, and details of the refinement of neutron-scattering data).
- [16] R. Lortz, Y. Wang, A. Demuer, P. H. M. Böttger, B. Bergk, G. Zwicknagl, Y. Nakazawa, and J. Wosnitza, *Phys. Rev. Lett.* **99**, 187002 (2007).
- [17] Y. Skourski, M. D. Kuz'min, K. P. Skokov, A. V. Andreev, and J. Wosnitza, *Phys. Rev. B* **83**, 214420 (2011).
- [18] B. Ouladdiaf, J. Archer, J. R. Allibon, P. Decapentrie, M. H. Lemée-Cailleau, J. Rodríguez-Carvajal, A. W. Hewat, S. York, D. Brau, and G. J. McIntyre, *J. Appl. Cryst.* **44**, 392 (2011).
- [19] L. Fuentes-Montero, P. Čermák, J. Rodríguez-Carvajal, and A. Filhol, doi: [10.13140/RG.2.1.4954.1202](https://doi.org/10.13140/RG.2.1.4954.1202) (<https://www.ill.eu/users/support-labs-infrastructure/software-scientific-tools/esmeralda/>).
- [20] V. Petříček, M. Dušek, and L. Palatinus, *Z. Kristallogr.* **229**, 345 (2014).
- [21] V. Petříček, M. S. Henriques, and M. Dušek, *Acta Phys. Pol. A* **130**, 848 (2016).
- [22] J. M. Perez-Mato, S. V. Gallego, E. S. Tasci, L. Elcoro, G. de la Flor, and M. I. Aroyo, *Annu. Rev. Mater. Res.* **45**, 217 (2015).
- [23] M. Reiffers, Y. G. Naidyuk, A. G. M. Jansen, P. Wyder, I. K. Yanson, D. Gignoux, and D. P. Schmitt, *Phys. Rev. Lett.* **62**, 1560 (1989).
- [24] A. R. Ball, D. Gignoux, F. E. Kayzel, D. Schmitt, and A. de Visser, *J. Magn. Magn. Mater.* **110**, 337 (1992).
- [25] F. Y. Zhang, D. Gignoux, D. Schmitt, J. J. M. Franse, F. E. Kayzel, N. H. Kim-Ngan, and R. J. Radwanski, *J. Magn. Magn. Mater.* **130**, 108 (1994).
- [26] M. D. Kuz'min, Y. Skourski, K. P. Skokov, and K. H. Müller, *Phys. Rev. B* **75**, 184439 (2007).
- [27] M. D. Kuz'min, Y. Skourski, K. P. Skokov, K. H. Müller, and O. Gutfleisch, *Phys. Rev. B* **77**, 132411 (2008).
- [28] E. Y. Chen, J. F. Dillon, Jr., and H. J. Guggenheim, *J. Appl. Phys.* **48**, 804 (1977).
- [29] N. V. Baranov, P. E. Markin, A. I. Kozlov, and E. V. Sinitsyn, *J. Alloys Compd.* **200**, 43 (1993).
- [30] N. V. Baranov, E. Bauer, R. Hauser, A. Calatanu, Y. Aoki, and H. Sato, *Eur. Phys. J. B* **16**, 67 (2000).
- [31] E. D. Mun, S. L. Bud'ko, H. Kob, G. J. Miller, and P. C. Canfield, *J. Magn. Magn. Mater.* **322**, 3527 (2010).
- [32] D. I. Gorbunov, M. S. Henriques, A. V. Andreev, A. Gukasov, V. Petříček, N. V. Baranov, Y. Skourski, V. Eigner, M. Paukov, J. Prokleška, and A. P. Gonçalves, *Phys. Rev. B* **90**, 094405 (2014).
- [33] D. I. Gorbunov, M. S. Henriques, A. V. Andreev, Y. Skourski, and M. Dušek, *J. Alloys Compd.* **634**, 115 (2015).
- [34] D. Gignoux and D. Schmitt, *Phys. Rev. B* **48**, 12682 (1993).
- [35] D. Gignoux and D. Schmitt, in *Handbook of Magnetic Materials*, edited by K. H. J. Buschow, Vol. 10 (Elsevier, Amsterdam, 1997), p. 239.
- [36] V. Petříček, J. Fuksa, and M. Dušek, *Acta Crystallogr. A* **66**, 649 (2010).
- [37] J. J. M. Franse and R. J. Radwanski, in *Handbook of Magnetic Materials*, edited by K. H. J. Buschow, Vol. 7 (Elsevier, Amsterdam, 1993), p. 307.
- [38] J. García Soldevilla, J. A. Blanco, J. Rodríguez Fernández, J. I. Espeso, J. C. Gómez Sal, M. T. Fernandez-Díaz, J. Rodríguez-Carvajal, and D. Paccard, *Phys. Rev. B* **70**, 224411 (2004).
- [39] P. Schobinger-Papamantellos, J. Rodríguez-Carvajal, and K. H. J. Buschow, *J. Alloys Compd.* **274**, 83 (1998).
- [40] P. Schobinger-Papamantellos, K. H. J. Buschow, C. Ritter, and L. Keller, *J. Magn. Magn. Mater.* **264**, 130 (2003).
- [41] P. Čermák, K. Prokeš, B. Ouladdiaf, M. Boehm, M. Kratochvílová, and P. Javorský, *Phys. Rev. B* **91**, 144404 (2015).
- [42] K. Prokeš, E. Muñoz-Sandoval, A. D. Chinchure, and J. A. Mydosh, *Phys. Rev. B* **78**, 014425 (2008).